PHYSICAL REVIEW B VOLUME 16, NUMBER 5 1 SEPTEMBER 1977

Interference parameters in γ-ray optics*

H. C. Goldwire, Jr.
Los Alamos Scientific Laboratory, Los Alamos, New Mexico 87544

J. P. Hannon
Physics Department, Rice University, Houston, Texas 77001
(Received 28 March 1977)

Calculations are given for the interference (or "screening") parameters $\xi(L\lambda)$ arising in low-energy γ-ray optics. In γ-ray emission, these parameters arise from the interaction of the emitted photon with the surrounding electron cloud of the atom, giving a phase shift to the emitted photon which depends on the multipolarity of the nuclear transition. In γ-ray absorption experiments, the parameters specify the effects of the interference between photoelectron and internal-conversion electron absorption, and the interference betweeen nonresonant scattering from the atomic electrons and resonant scattering from the nucleus. These interference effects give rise to a dispersion term in the total cross section, thereby producing a small asymmety in the absorption spectrum and slightly shifting the center of the absorption line. These effects can be very important in determining precise isomer shifts and in analyzing Mössbauer tests of time-reversal invariance. We present calculated screening parameters for $E1$, $M1$, and $E2$ γ-ray transitions, and we examine their dependences on the nuclear charge and the γ-ray energy. We compare the results with the available experimental determinations.

I. INTRODUCTION

In connection with the time-reversal invariance experiments of Kistner,[1] and of Atac, Chrisman, Debrunner, and Frauenfelder,[2] it was pointed out[3] that there is a "dispersion" term in the absorption spectrum of Mössbauer γ rays [proportional to $2\xi(L\lambda)x/(x^2+1)$, where x is the deviation from resonance and $\xi(L\lambda)$ is the "interference" or "screening" parameter] which represents the interference between the processes of nuclear resonance absorption followed by internal conversion and the direct (nonresonant) photoelectric absorption by the atomic electrons. A large dispersion term was subsequently noted by Sauer, Matthias, and Mössbauer[4] in the absorption spectrum of ^{181}Ta. This was explained theoretically by Trammell and Hannon[5,6] and independently by Kagan, Afanas'ev, and Voitovetskii.[7] At the time, it was felt that the dispersion was anomalously large in this case because the nuclear resonance was $E1$, giving a large interference with the photoelectric absorption, which is also predominantly $E1$. (We will see later that this reasoning is incorrect, and that very large effects can also be expected for low-energy $E2$ transitions.)

Subsequent observations of the interference in the remaining known $E1$ Mössbauer transitions were obtained by Gorobchenko *et al.*,[8] and by Henning, Bähre, and Kienle.[9] The dispersion in a number of Mössbauer absorbers of higher multipolarity ($E2$ and $M1/E2$) has been observed by Wagner and collaborators,[10] and a careful determination of the screening in the 77.3-keV $E2/M1$ transition of ^{197}Au has been obtained by Erickson, Prince, and Roberts.[11] Very recently, a large dispersion has been observed by Pfeiffer[12] in the absorption spectrum of the 13.5-keV $E2$ transition of ^{73}Ge.

The interference between photoelectrons and conversion electrons can also be detected in direct observations of the ejected electrons as discussed by Afanas'ev and Kagan,[13] and such measurements have been carried out by several groups.[14-16] Similarly, the interference between nonresonant Rayleigh scattering from the electrons and coherent elastic resonant scattering from the nucleus, which, as discussed below, also contributes to the interference parameters $\xi(L\lambda)$, can be detected by observing the scattered γ rays, as was first done in the early experiments of Black, Moon, and co-workers.[17-19]

A theoretical treatment of the effect of the interference on Mössbauer relaxation spectra has recently been given by Hartmann-Boutron and Spanjaard.[20]

These interference effects can be very important in determining precise isomer shifts[11,21] and in analyzing tests of time-reversal invariance involving γ transitions.[3,22-24] This effect is also of interest from the atomic physics standpoint because, e.g., for an $M1$ or $E2$ Mössbauer absorber the dispersion term is proportional to the $M1$ or $E2$ *partial amplitudes* for atomic photoelectric absorption. Now, whereas in the energy range involved the photoelectric cross section is nearly all $E1$, with the partial $M1$ or $E2$ *cross sections* being very small, the dispersion term (being pro-

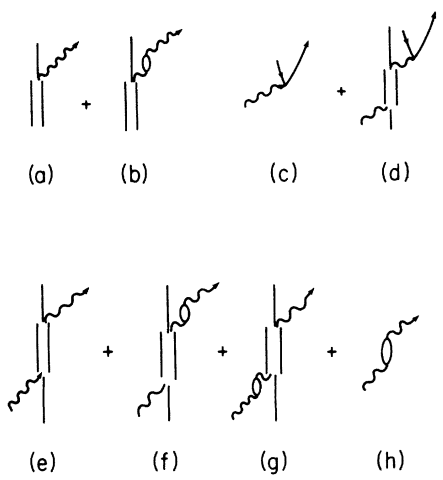

FIG. 1. Feynman diagrams representing emission (a) and (b), absorption (c) and (d), and scattering processes (e)–(h).

portional to amplitudes) is proportional to the geometric mean of the large nuclear resonance cross section and the relevant partial photoelectric atomic cross section, and thus effectively picks out and greatly amplifies this multipole partial cross section.

Thus it is important to have theoretical calculations of the interference parameters $\xi(L\lambda)$, and the purpose of this paper is to present such calculations. In particular, we calculate the interference parameters for $E1$, $M1$, and $E2$ γ-ray transitions in the low energy γ-ray region (10–200 kev), for values of the nuclear charge Z ranging from 10 to 100.

We have divided the paper into six sections: In Sec. II, we summarize the theory, and in Sec. III we give the theoretical expressions for the interference parameters $\xi(L\lambda)$. The results of our calculations are presented in Sec. IV, and we make a comparison with the available experimental determinations in Sec. V. In Sec. VI we summarize our main results.

II. THEORY

These "interference" or "screening" parameters arise not only in *absorption* experiments, such as discussed in the previous section, but also in *emission* and *scattering* experiments.

A. Emission

As discussed in Refs. 3, 5, and 6, when a γ ray is emitted from a nucleus, the scattering of the photon by the surrounding electron cloud of the atom gives rise to a complex index of refraction for passage of the photon through the electron cloud. In effect, the radiation emitted by the nuclear transition induces multipole currents in the electron cloud, and the radiation emitted by these induced electronic currents interferes with the primary radiation from the nucleus. This is indicated schematically in Fig. 1, where Fig. 1(a) represents the emission from a bare nucleus and Fig. 1(b) represents the first-order scattering contribution. In analogy to the screening of a static charge impurity by a surrounding electron gas, the scattering contribution of 1(b) gives a dynamical screening of the nuclear transition current by the surrounding electron cloud.

For a pure $L\lambda$ multipole nuclear transition[$L,0 \equiv M(L)$ = magnetic 2^L pole; $L,1 \equiv E(L)$ = electric 2^L pole], the bare nuclear transition current for emission of a photon $|\vec{k}_0\rangle$ is

$$\vec{J}_\perp^{fn}(-\vec{k}_0) = \langle f| \int d\vec{x}\, \vec{J}_\perp(\vec{x}) e^{-i\vec{k}_0\cdot\vec{x}} |n\rangle$$

$$= C(j_0 L j_n; m_0 M m_n) e^{i\eta_{L\lambda}}$$

$$\times [\lambda_0 \Gamma_\gamma(L\lambda)]^{1/2} \vec{Y}_{LM}^{(\lambda)}(\vec{k}_0)\,, \qquad (1)$$

where Γ_γ is the radiative width for the transition, λ_0 is the photon wavelength, $\eta_{L\lambda}$ gives the phase of the reduced nuclear matrix element for emission, $\vec{Y}_{LM}^{(\lambda)}(\vec{k}_0)$ is a vector spherical harmonic, j_0 and j_n give the angular momentum of the ground and excited nuclear levels respectively, m_0 and m_n give the z projection of j in the ground and excited levels, $M = m_n - m_0$, and, finally, the notation for the Clebsch-Gordan coefficients is that of Rose.[25]

The effect of the electronic scattering is to replace the bare nuclear current $\vec{J}^{fn}$ by the "screened" nuclear current $\vec{J}^{fn}$,

$$\vec{J}_\perp^{fn}(-\vec{k}_0) = \vec{J}_\perp^{fn}(-\vec{k}_0)[1 + \delta(L\lambda) + i\xi(L\lambda)]\,, \qquad (2)$$

$\vec{J}^{fn}$ being just the bare current multiplied by the screening factor $n(L\lambda) = 1 + \delta(L\lambda) + i\xi(L\lambda)$. The parameter $\delta + i\xi$ will be referred to as the "screening parameter," or, alternatively, as the "interference parameter."

The contribution $\delta(L\lambda)$ gives the effect of the induced electronic currents which are in phase, or 180° out of phase, with the nuclear currents. Typically, $\delta(L\lambda)$ values are small ($\approx 10^{-5}$–$10^{-2} \ll 1$), and in emission give only a small correction to the nuclear radiation width which can generally be neglected. On the other hand, the imaginary part $i\xi(L\lambda)$, although small ($\approx 10^{-3}$–10^{-1} rad), gives a phase shift to the emitted multipole wave which is of importance in analyzing the results of T-invariance experiments.[3,6,22-24]

B. Scattering

Screening also affects γ-ray scattering processes, as indicated schematically in Fig. 1. Figure 1(e) represents the scattering of a γ ray by a "bare" nucleus, while in Fig. 1(f) the photon scattered by the nucleus is then scattered by the electron cloud, and in Fig. 1(g) the photon scatters from the electrons before scattering from the nucleus. Finally, Fig. 1(h) represents the purely electronic scattering processes.

The scattering from the nucleus is a combined absorption-emission process, and the effect of the screening process Fig. 1(f) is again to modify the "emission current" by the screening factor $1+\delta(L\lambda)+i\xi(L\lambda)$ as given in Eq. (2), and similarly the effect of the screening process [Fig. 1(g)] is to modify the "absorption current" by the same screening factor.[3] Then the overall effect of the screening processes in γ-ray scattering is to modify the nuclear scattering amplitude by the factor $(1+\delta+i\xi)^2 \simeq 1+2\delta(L\lambda)+2i\xi(L\lambda)$. In particular, the coherent elastic scattering amplitude for scattering an incident $|\vec{k}_0, \hat{e}_f\rangle$ photon into a $|\vec{k}_f, \hat{e}_f\rangle$ photon is then

$$f(\vec{k}_f, \hat{e}_f; \vec{k}_0, \hat{e}_0) = f_n(\vec{k}_f, \hat{e}_f; \vec{k}_0, \hat{e}_0) + f_e(\vec{k}_f, \hat{e}_f; \vec{k}_0, \hat{e}_0), \tag{3}$$

where the amplitude for resonant scattering from the nucleus is

$$f_n(\vec{k}_f, \hat{e}_f; \vec{k}_0, \hat{e}_0) = \frac{4\pi\lambda\!\!\!^{-}_0}{2j_0+1}\left(\frac{\Gamma_\gamma(L\lambda)}{\Gamma}\right) e^{-k^2\langle u^2\rangle}[1+2\delta(L\lambda)+2i\xi(L\lambda)] \times \sum_{m_0}\sum_{M=-L}^{+L} \frac{C^2(j_0 L j_n; m_0 M)}{[x(m_0 M)-i]}\, \hat{e}_f^* \cdot \vec{Y}_{LM}^{(\lambda)}(\vec{k}_f)\vec{Y}_{LM}^{(\lambda)}(\vec{k}_0)^* \cdot \hat{e}_0 , \tag{4}$$

and the amplitude for nonresonant scattering from the electrons (taking into account the leading Thomson and photoelectric contributions) is

$$f_e(\vec{k}_f, \hat{e}_f; \vec{k}_0, \hat{e}_0) = \hat{e}_f^* \cdot \hat{e}_0 e^{-1/2(\vec{k}_f - \vec{k}_0)^2\langle u^2\rangle} \times [-(e^2/mc^2)F(\theta) + i(k_0/4\pi)\sigma_e]. \tag{5}$$

In Eq. (4),

$$x(m_0 M) = 2[E(j_n, m_0+M) - E(j_0, m_0) - \hbar\omega_0]/\Gamma$$

gives the deviation from resonance in units of the halfwidth, and the factor $e^{-k^2\langle u^2\rangle}$ is the usual Mössbauer factor. In Eq. (5),

$$F(\theta) = \langle E_0 | \sum_j e^{i(\vec{k}_0 - \vec{k}_f)\cdot\vec{x}_j} | E_0\rangle$$

is the electronic form factor for the atom, $\exp[-1/2 \times (\vec{k}_f - \vec{k}_0)^2\langle u^2\rangle]$ is the Debye-Waller phonon factor, and σ_e is the total cross section for the processes of photoelectric absorption and of elastic and inelastic γ-ray scattering from the atomic electrons.

C. Absorption

The effect of the screening processes on absorption experiments can be obtained immediately from Eqs. (3)–(5). The transmitted beam in such experiments is determined by the total cross section, which from the optical theorem is given by

$$\sigma = (4\pi/k_0)\,\mathrm{Im} f(\vec{k}_0, \hat{e}_0; \vec{k}_0, \hat{e}_0) = \sigma_n + \sigma_e , \tag{6}$$

where the total cross section for resonant scattering and absorption is given by

$$\sigma_n = \frac{16\pi^2\lambda\!\!\!^{-}_0{}^2}{2j_0+1} e^{-k^2\langle u^2\rangle} \frac{\Gamma_\gamma}{\Gamma} \sum_{m_0 M}\sum C^2(j_0 L j_n; m_0 M) \left| Y_{LM}^{(\lambda)*}(\vec{k}_0)\cdot\hat{e}_0\right|^2 \left(\frac{1+2\xi(L\lambda)x(m_0 M)}{x(m_0 M)^2+1}\right). \tag{7}$$

Here, as in the emission processes, we are able to ignore the real part of the screening factor $\delta(L\lambda)$, since it occurs only in the combination $1+2\delta$ and δ is much less than unity. In the limit of no Zeeman splitting, the resonant cross section becomes

$$\sigma_n = \sigma_0[(1+2\xi x)/(x^2+1)], \tag{8}$$

where σ_0 is the total cross section at exact resonance,

$$\sigma_0 = 2\pi\lambda\!\!\!^{-}_0{}^2 \left(\frac{2j_n+1}{2j_0+1}\right) e^{-k^2\langle u^2\rangle}\left(\frac{\Gamma_\gamma}{\Gamma}\right), \tag{9}$$

and $x = 2[E(j_n) - E(j_0) - \hbar\omega_0]/\Gamma$ is the deviation from resonance.

Equations (6)–(9) give the main results for absorption experiments. In particular, from (7) and (8) we see that the screening gives a small disper-

sion term $[2\xi x/(x^2+1)]\sigma_0$ to the total cross section. The effect of this contribution is to give a small asymmetry to the Mössbauer absorption spectrum and to shift the minimum of the spectrum from $x=0$ to $x\simeq\xi$. As noted before, although the screening effect is small, the induced dispersion can be very important in isotope shift measurements[11,21] and in T-invariance experiments.[3,6,22-24]

For these absorption experiments, the imaginary part of the screening parameter, $\xi(L\lambda)$, which gives the important dispersion term, arises from the interference between coherent competing processes and for this reason we also refer to ξ as the "interference parameter."

As discussed in Refs. 3 and 5–7, and even earlier by Lipkin and Tassie,[26] the dominant contribution to ξ arises from the interference between direct (nonresonant) photoelectric absorption and resonant absorption by the nucleus followed by conversion. These two absorption processes are shown schematically in Figs. 1(c) and 1(d). Since both processes have the same initial and final states (assuming no nuclear spin flip), they are quantum-mechanically coherent and hence interfere. This contribution to $\xi(L\lambda)$ will be referred to as "conversion screening."

A second contribution to ξ arises from the interference between resonant scattering from the nucleus and nonresonant scattering from the atomic electrons and these two processes are shown schematically in Figs. 1(e) and 1(h), respectively. We will refer to this contribution as "Rayleigh screening."[27] In most cases the primary contribution to ξ is from conversion screening, but we will see that in a few isolated cases Rayleigh screening is dominant.

The magnitude of the screening effects is dependent on the multipolarity of the Mössbauer transition, but not as strongly as one might expect. In the case of Rayleigh screening the strongest effect occurs if the Mössbauer transition is $E1$. This occurs because the Rayleigh scattering from the electrons is primarily $E1$, so that if the resonant transition is $M1$ or higher, the final photon states are almost orthogonal, i.e., $\int f_n^* f_e\, d\Omega \simeq 0$, and it is only the small admixture of higher multipole orders in the Rayleigh scattering which lead to a nonzero Rayleigh screening contribution ξ_R.

In the case of conversion screening we might expect a similar result since the photoelectric transition is also primarily $E1$. However, this conclusion is not correct and in particular we will see that the interference parameters ξ for $E2$ transitions are often larger than those for $E1$ transitions. This occurs because for an $L\lambda$ multipole nuclear transition, the interference parameter $\xi(L\lambda)$ is proportional to $[\sigma'_{pe}(L\lambda)\sigma_{ic}(L\lambda)]^{1/2}$, where $\sigma'_{pe}(L\lambda)$ is the partial cross section for the $L\lambda$ multipole contribution to photoelectric absorption and $\sigma_{ic}(L\lambda)$ is the cross section for internal-conversion absorption at resonance. For an $E2$ transition, the photoelectric partial cross section $\sigma'_{pe}(E2)$ is much less than the $E1$ contribution, i.e., $\sigma'_{pe}(E2)\ll\sigma'_{pe}(E1)$, but on the other hand internal conversion is much stronger for an $E2$ transition than for a corresponding $E1$ transition, so that $\sigma_{ic}(E2)\gg\sigma_{ic}(E1)$. We will see that this amplification of the internal conversion cross section just offsets the reduction of the photoelectric partial cross section, so that in fact $\xi(E2)\sim\xi(E1)$. As noted earlier, such a large $E2$ dispersion has very recently been observed by Pfeiffer in the 13.5-keV ^{73}Ge transition.[12]

III. THEORETICAL EXPRESSIONS FOR THE SCREENING

The explicit expressions for the screening factors have been developed in three previous papers,[3,5,6] and here we summarize the results.

A. Conversion screening

For ML and EL γ-ray transitions, the conversion screening contributions are given, respectively, by

$$\delta(ML)+i\xi(ML)=-\pi\alpha k[L(L+1)(2L+1)]^{-1}\times\sum_{\mu\mu'}B_{\mu\mu'}r_{\mu\mu'}(m)R_{\mu\mu'}(m), \tag{10}$$

$$\delta(EL)+i\xi(EL)=-\pi\alpha k[L(L+1)(2L+1)]^{-1}\times\sum_{\mu\mu'}C_{\mu\mu'}r_{\mu\mu'}(e)R_{\mu\mu'}(e). \tag{11}$$

Here the notation is that of Rose[28]: $k=\hbar\omega_0/mc^2$, $\alpha=\frac{1}{137}$, and the $R_{\mu\mu'}$ are the usual internal-conversion (ic) matrix elements,

$$R_{\mu\mu'}(m)=\int_0^\infty h_L^{(1)}(kr)[f_\mu(pr)g_{\mu'}+g_\mu(pr)f_{\mu'}]r^2\,dr, \tag{12}$$

$$\begin{aligned}R_{\mu\mu'}(e)&=(\mu'-\mu)\int_0^\infty h_{L-1}^{(1)}(kr)[f_\mu(pr)g_{\mu'}+g_\mu(pr)f_{\mu'}]r^2\,dr\\&\quad-L\int_0^\infty h_{L-1}^{(1)}(kr)[f_\mu(pr)g_{\mu'}-g_\mu(pr)f_{\mu'}]r^2dr\\&\quad+L\int^\infty h_L^{(1)}(kr)[f_\mu(pr)f_{\mu'}+g_\mu(pr)g_{\mu'}]r^2\,dr.\end{aligned} \tag{13}$$

In (12) and (13), $g_{\mu'}$ and $f_{\mu'}$ are the upper and lower component radial wave functions for the bound state, and $g_\mu(pr)$ and $f_\mu(pr)$ are the radial wave functions for the continuum state. The $h_L^{(1)}$'s are spherical Hankel functions of the first type. In (11),

the coefficients $B_{\mu\mu'}$ and $C_{\mu\mu'}=B_{-\mu\mu'}/(\mu-\mu')^2$ are given in Table b of Ref. 28. Finally, the integrals $r_{\mu\mu'}(m)$ and $r_{\mu\mu'}(e)$ are given by expressions (12) and (13) with each spherical Hankel function $h_L^{(1)}(kr)$ replaced by the corresponding spherical Bessel function $j_L(kr)$. However, since $h_L^{(1)}(y)=j_L(y)+in_L(y)$, where both the spherical Bessel function j_L and the spherical Neuman function $n_L(y)$ are real, then *if* the continuum radial wave functions $g_\mu(pr)$, $f_\mu(pr)$ are taken as *real* standing waves (as is customary in internal-conversion calculations), then $r_{\mu\mu'}(m)$ and $r_{\mu\mu'}(e)$ are given simply by the real parts of $R_{\mu\mu'}(m)$ and $R_{\mu\mu'}(e)$:

$$r_{\mu\mu'}(m)=\mathrm{Re}\{R_{\mu\mu'}(m)\},$$
$$r_{\mu\mu'}(e)=\mathrm{Re}\{R_{\mu\mu'}(e)\}. \tag{14}$$

Thus in order to calculate the conversion screening parameter, one only needs the tabulated or calculated internal conversion matrix elements $R_{\mu\mu'}$ and Eqs. (10), (11), and (14). Unfortunately, although there are very extensive tables of internal conversion coefficients, the tables of ic matrix elements are very limited. The most extensive tables that we are aware of are the K-shell results of Rose,[28] and the K- and L-shell results of Band, Listengarten, and Sliv.[29,30] For some cases we have utilized these tables, but for most cases it was necessary to calculate the ic matrix elements directly.

Finally, a useful approximate expression for the conversion screening for a pure $(L\lambda)$ multipole transition is given by[5,7]

$$\xi_c(L\lambda)=\epsilon[\alpha(L\lambda)\sigma'_{pe}(L\lambda)/(4L+2)\pi\lambda\!\!\!^{-2}_0]^{1/2}, \tag{15}$$

where $\alpha(L\lambda)$ is the internal conversion coefficient, λ_0 is the wave length of the incident γ ray, and $\sigma'_{pe}(L\lambda)$ is the *partial* cross section for the EL or ML contribution to photoelectric absorption [Eqs. (A1) and (A2)]. ϵ is a positive or negative real number which has an absolute value somewhat less than one. It differs from unity because both $\alpha(L\lambda)$ and $\sigma'_{pe}(L\lambda)$ are the sums of squares of amplitudes ($\sum_\mu|R_{\mu\mu'}|^2$ and $\sum_\mu|r_{\mu\mu'}|^2$, respectively), whereas ξ is proportional to the sum of the product of the photoelectric times the internal conversion amplitude $\sum_\mu r_{\mu\mu'}R_{\mu\mu'}$.

B. Rayleigh screening

In the 1-Å region, the dominant γ-ray scattering process from the atomic electrons which can interfere coherently with the resonant scattering from the nucleus is the Thomson scattering arising from the A^2 interaction. For ML and EL γ-ray transitions, the Thomson contribution to the Rayleigh screening parameter is given by[31]

$$\delta_R(ML)+i\xi_R(ML)=-iZk_0r_0\langle j_L(k_0r)h_L^{(1)}(k_0r)\rangle, \tag{16}$$

$$\delta_R(EL)+i\xi_R(EL)=-iZk_0r_0\left\langle\left(\frac{L+1}{2L+1}\right)j_{L-1}(k_0r)h_{L-1}^{(1)}(k_0r)+\left(\frac{L}{2L+1}\right)j_{L+1}(k_0r)h_{L+1}^{(1)}(k_0r)\right\rangle. \tag{17}$$

Here Z is the nuclear charge, $r_0=e^2/mc^2$ and the brackets $\langle\ \rangle$ indicate an average of the corresponding function over the ground-state charge distribution $\rho(r)$, e.g.,

$$\langle j_Lh_L^{(1)}\rangle=\frac{1}{Z}\int_0^\infty\rho(r)j_L(k_0r)h_L^{(1)}(k_0r)r^2\,dr.$$

In analogy to Eq. (15), a useful expression for the Thomson contribution to Rayleigh screening is given by[5]

$$\xi_R(L\lambda)=-[\sigma_R(L\lambda)/(4L+2)\pi\lambda\!\!\!^{-2}_0]^{1/2}, \tag{18}$$

where $\sigma_R(L\lambda)$ is the partial cross section for the EL or ML contribution to Thomson scattering [Eqs. (A3) and (A4)].

In addition to the Thomson contribution to Rayleigh screening, there is also interference between the resonant scattering from the nucleus and the scattering from the electrons arising from virtual transitions to unoccupied excited states induced by the $\vec{j}\cdot\vec{A}$ interaction (the anomalous scattering and dispersion of x rays[32]), giving a Rayleigh screening contribution

$$\xi'_R(\Gamma\lambda)=-\frac{ke^2}{4\pi}PV\sum_{E_p}[\langle E_0|\vec{\alpha}\cdot\vec{A}^{(\lambda)}_{LM}{}^*|E_p\rangle\langle E_p|\vec{\alpha}\cdot\vec{A}^{(\lambda)}_{LM}|E_0\rangle(E_0-E_p+k)^{-1}+\langle E_0|\vec{\alpha}\cdot\vec{A}^{(\lambda)}_{LM}|E_p\rangle\langle E_p|\vec{\alpha}\cdot\vec{A}^{(\lambda)}_{LM}{}^*|E_0\rangle(E_0-E_p-k)^{-1}]$$
$$=\frac{2}{\pi}PV\sum_{E_p}\delta(L\lambda)\frac{(E_0-E_p)}{(E_0-E_p)^2-k^2}. \tag{19}$$

Here, we have assumed the atom is spherical (closed electronic shells), E_0 is the ground electronic state, and the sum over E_p is over unoccupied bound states and continuum electronic states, taking the principal value at the singularity $E_p = E_0 + k$. Finally, $\delta(L\lambda)$ is given by the real part of Eqs. (10), (11).

If the γ-ray energy is well removed from the x-ray absorption edges, the anomalous scattering is much smaller than the Thomson scattering, and ξ_R' can be neglected. However, if E_γ is within a few eV of an absorption edge, the anomalous scattering will be quite pronounced, and (19) would then give a significant correction to the Thomson contribution to ξ_R.

Finally, we note that there is also appreciable Compton scattering of γ rays, particularly in the region $E_\gamma \gg 100$ keV, but Compton scattering is not coherent with the resonant scattering from the nucleus considered above since the final electronic states will be different in the two cases. Hence Compton scattering makes no direct contribution to Rayleigh screening. However, there will be a "Compton screening" contribution to $\xi(L\lambda)$ which arises from the interference between direct Compton scattering and the coherent process of resonant nuclear absorption followed by deexcitation by emission of a lower energy photon and the "simultaneous" ejection of an atomic electron. (From a relativistic point of view, this Compton deexcitation will be sequential scattering process rather than a simultaneous process.) It should be interesting to investigate this process in its own right, but in the *low-energy* γ-ray region that we are considering, the cross sections for photoelectric absorption and elastic scattering dominate the Compton scattering cross section, so the Compton screening contribution to ξ should be negligible.

IV. RESULTS

A. Conversion screening

When the γ-ray energy is sufficiently high that K-shell transitions are possible, then the dominant contribution to the conversion screening parameter ξ_c comes from the K shell, with the contributions from the outer shells being about 20% as large.

As noted previously, to calculate $\delta + i\xi$, it is only necessary to calculate the ic matrix elements $R_{\mu\mu'}$. For the K shell, there are very few tabulations of the $R_{\mu\mu'}$ in the energy range of interest to Mössbauer γ-ray optics. In order to avoid interpolation uncertainties and the problem of extrapolation beyond existing tables, we calculated the K-shell matrix elements directly using unscreened, point nucleus, relativistic wave functions. As discussed by Rose,[28,33] screening is relatively unimportant for K-shell results. A direct comparison of the unscreened K-shell ic matrix elements of Rose[28] with the screened calculations of Band, Listengarten, and Sliv[29] shows that the screening changes the magnitude of $R_{\mu\mu'}$ by at most a few percent, and hence our determinations of the K-shell contribution ξ_K should be correct to within a few percent.

For the L shell, such calculations are more involved and much more sensitive to screening. Here we utilized the L-shell tables of Band, Listengarten, and Sliv.[30] Although these tables are restricted to relatively high Z, they do cover the energy region of interest.

As discussed in Sec. II, the quantity of importance is the imaginary contribution ξ. In Table I we tabulate ξ_K, the K-shell contribution to ξ_c, for $E1$, $M1$, and $E2$ multipolarities, for γ-ray energies ranging from 10–200 keV, and for Z ranging from 10 to 90. In Tables II and III we tabulate ξ_L, the L-shell contribution to ξ_c, for the same multipolarities, for E_γ ranging from ~25–200 keV and Z ranging from 49 to 92.

To better demonstrate the nature of these results, in Figs. 2 and 3 we give plots of ξ_K and ξ_L as functions of E_γ and Z. In Fig. 2(a) we plot the K-shell contribution to ξ_c (Table I) as a function of E_γ for an intermediate value of Z ($Z = 40$), and a high Z ($Z = 83$). We see that ξ_K usually decreases rapidly with increasing E_γ. This is to be expected since both the internal conversion effect and the photoelectric effect decrease as E_γ increases. However, this behavior is not always followed, as we see in the case of $\xi_K(E2)$ for $Z = 83$. In this case, as the energy increases and the photoelectric effect becomes less $E1$ in character, the $E2$ contribution in fact initially increases with E_γ. As already noted in Eq. (15), $\xi_K(E2)$ depends on the partial cross section $\sigma'_{pe}(E2)$ and it is the peaking of this partial cross section which produces the behavior shown in Fig. 2(a).

We also note in Fig. 2(a) that for $Z = 40$, the $E1$ and $E2$ K-shell conversion screening factors are the same order of magnitude, with $\xi_K(E2)$ in fact being larger in the high energy region, and also that $\xi_K(M1)$ is greatly suppressed relative to $\xi_K(E1)$ and $\xi_K(E2)$.

The reason for the rough equality of $\xi_K(E1)$ and $\xi_K(E2)$ was explained in Sec. II and can now be seen explicitly from expressions (11), (13), and (14): For an $E1$ transition, $R_{\mu\mu'}(E1)$ and $r_{\mu\mu'}(E1)$ involve matrix elements of $h_1^{(1)}(kr)$ and $j_1(kr)$ respectively, while for an $E2$ transition $R_{\mu\mu'}(E2)$ and $r_{\mu\mu'}(E2)$ involve $h_2^{(1)}(kr)$ and $j_2(kr)$, respectively. For the K shell, we generally have $kr \ll 1$ so that $h_L^{(1)}(kr) \propto (kr)^{-(L+1)}$ and $j_L(kr) \propto (kr)^L$. Thus in

TABLE I. K-shell contribution to conversion screening parameter.

E_γ (keV)	$Z=10$	$Z=20$	$Z=30$	$Z=40$	$Z=50$	$Z=60$	$Z=70$	$Z=80$	$Z=90$	$Z=100$
								$\xi_K(E1)$		
10	−5.48(−3)	−4.21(−2)								
20	−1.23(−3)	−1.11(−2)	−3.47(−2)							
30	−4.95(−4)	−4.87(−3)	−1.62(−2)	−3.51(−2)						
40	−2.57(−4)	−2.65(−3)	−9.23(−3)	−2.08(−2)	−3.71(−2)					
60	−9.96(−5)	−1.10(−3)	−4.03(−3)	−9.56(−3)	−1.79(−2)	−2.87(−2)				
80	−5.02(−5)	−5.77(−4)	−2.19(−3)	−5.36(−3)	−1.03(−2)	−1.72(−2)	−2.55(−2)			
100	−2.93(−5)	−3.46(−4)	−1.35(−3)	−3.37(−3)	−6.66(−3)	−1.13(−2)	−1.72(−2)	−2.41(−2)		
120	−1.88(−5)	−2.27(−4)	−9.01(−4)	−2.29(−3)	−4.60(−3)	−7.95(−3)	−1.24(−2)	−1.77(−2)		
140	−1.29(−5)	−1.58(−4)	−6.38(−4)	−1.65(−3)	−3.35(−3)	−5.87(−3)	−9.26(−3)	−1.35(−2)	−1.82(−2)	
160	−9.27(−6)	−1.16(−4)	−4.71(−4)	−1.23(−3)	−2.53(−3)	−4.49(−3)	−7.17(−3)	−1.06(−2)	−1.46(−2)	
180	−6.93(−6)	−8.75(−5)	−3.61(−4)	−9.51(−4)	−1.98(−3)	−3.54(−3)	−5.71(−3)	−8.53(−3)	−1.19(−2)	−1.56(−2)
200	−5.34(−6)	−6.81(−5)	−2.83(−4)	−7.54(−4)	−1.58(−3)	−2.85(−3)	−4.65(−3)	−7.02(−3)	−9.92(−3)	−1.32(−2)
								$\xi_K(M1)$		
10	−1.98(−6)	−2.88(−5)								
20	−1.46(−6)	−2.17(−5)	−1.06(−4)							
30	−1.22(−6)	−1.82(−5)	−9.03(−5)	−2.86(−4)						
40	−1.07(−6)	−1.61(−5)	−7.99(−5)	−2.56(−4)	−6.47(−4)					
60	−8.87(−7)	−1.34(−5)	−6.67(−5)	−2.15(−4)	−5.52(−4)	−1.24(−3)				
80	−7.75(−7)	−1.17(−5)	−5.84(−5)	−1.89(−4)	−4.87(−4)	−1.10(−3)	−2.32(−3)			
100	−6.96(−7)	−1.05(−5)	−5.25(−5)	−1.70(−4)	−4.39(−4)	−9.99(−4)	−2.12(−3)	−4.37(−3)		
120	−6.37(−7)	−9.63(−6)	−4.81(−5)	−1.56(−4)	−4.02(−4)	−9.16(−4)	−1.95(−3)	−4.03(−3)		
140	−5.91(−7)	−8.93(−6)	−4.46(−5)	−1.44(−4)	−3.72(−4)	−8.49(−4)	−1.81(−3)	−3.75(−3)	−7.99(−3)	
160	−5.53(−7)	−8.36(−6)	−4.17(−5)	−1.35(−4)	−3.48(−4)	−8.93(−4)	−1.69(−3)	−3.51(−3)	−7.49(−3)	
180	−5.22(−7)	−7.88(−6)	−3.92(−5)	−1.27(−4)	−3.27(−4)	−7.45(−4)	−1.59(−3)	−3.30(−3)	−7.05(−3)	−1.67(−2)
200	−4.95(−7)	−7.47(−6)	−3.72(−5)	−1.20(−4)	−3.09(−4)	−7.04(−4)	−1.50(−3)	−3.12(−3)	−6.67(−3)	−1.58(−2)
								$\xi_K(E2)$		
10	−7.06(−3)	−3.30(−2)								
20	−1.72(−3)	−1.23(−2)	−2.42(−2)							
30	−7.20(−4)	−5.97(−3)	−1.50(−2)	−1.96(−2)						
40	−3.80(−4)	−3.44(−3)	−9.72(−3)	−1.57(−2)	−1.49(−2)					
60	−1.51(−4)	−1.51(−3)	−4.80(−3)	−9.22(−3)	−1.25(−2)	−1.14(−2)				
80	−7.73(−5)	−8.19(−4)	−2.78(−3)	−5.79(−3)	−8.87(−3)	−1.04(−2)	−8.47(−3)			
100	−4.55(−5)	−5.02(−4)	−1.78(−3)	−3.89(−3)	−6.38(−3)	−8.30(−3)	−8.43(−3)	−5.70(−3)		
120	−2.94(−5)	−3.34(−4)	−1.22(−3)	−2.76(−3)	−4.72(−3)	−6.54(−3)	−7.37(−3)	−6.31(−3)		
140	−2.02(−5)	−2.35(−4)	−8.76(−4)	−2.04(−3)	−3.60(−3)	−5.20(−3)	−6.24(−3)	−5.98(−3)	−3.93(−3)	
160	−1.46(−5)	−1.72(−4)	−6.55(−4)	−1.55(−3)	−2.81(−3)	−4.19(−3)	−5.24(−3)	−5.38(−3)	−4.08(−3)	
180	−1.09(−5)	−1.31(−4)	−5.04(−4)	−1.22(−3)	−2.24(−3)	−3.42(−3)	−4.42(−3)	−4.75(−3)	−3.91(−3)	−1.73(−3)
200	−8.40(−6)	−1.02(−4)	−3.99(−4)	−9.75(−4)	−1.82(−3)	−2.83(−3)	−3.74(−3)	−4.17(−3)	−3.62(−3)	−1.80(−3)

TABLE II. L-shell contribution to conversion screening parameter.[a]

E_γ (keV)	$Z=49$	$Z=53$	$Z=57$	$Z=61$	$Z=65$	$Z=69$	Multipolarity
25.6	−1.08(−2)	−1.39(−2)	−1.73(−2)	−2.13(−2)	−2.61(−2)	−3.14(−2)	$\xi_L(E1)$
51.1	−2.94(−3)	−3.83(−3)	−4.81(−3)	−6.06(−3)	−7.43(−3)	−8.96(−3)	
76.7	−1.28(−3)	−1.70(−3)	−2.19(−3)	−2.78(−3)	−3.47(−3)	−4.22(−3)	
102.2	−7.08(−4)	−9.49(−4)	−1.23(−3)	−1.55(−3)	−1.95(−3)	−2.40(−3)	
153.3	−3.07(−4)	−4.11(−4)	−5.48(−4)	−6.94(−4)	−8.65(−4)	−1.09(−3)	
204.4	−1.66(−4)	−2.30(−4)	−3.08(−4)	−3.94(−4)	−4.86(−4)	−6.10(−4)	
25.6	−6.46(−5)	−1.06(−4)	−1.59(−4)	−2.25(−4)	−3.15(−4)	−4.14(−4)	$\xi_L(M1)$
51.1	−7.75(−5)	−1.05(−4)	−1.39(−4)	−1.84(−4)	−2.42(−4)	−3.25(−4)	
76.7	−5.85(−5)	−8.25(−5)	−1.15(−4)	−1.56(−4)	−2.13(−4)	−2.85(−4)	
102.2	−4.85(−5)	−7.17(−5)	−1.03(−4)	−1.41(−4)	−1.86(−4)	−2.51(−4)	
153.3	−3.74(−5)	−5.50(−5)	−7.71(−5)	−1.05(−4)	−1.38(−4)	−1.86(−4)	
204.4	−3.22(−5)	−4.97(−5)	−7.07(−5)	−9.53(−5)	−1.26(−4)	−1.68(−4)	
25.6	−4.57(−3)	−4.85(−3)	−3.58(−3)	−3.35(−3)	−7.20(−4)	+3.40(−3)	$\xi_L(E2)$
51.1	−2.23(−3)	−2.61(−3)	−2.80(−3)	−3.15(−3)	−3.19(−3)	−2.79(−3)	
76.7	−1.16(−3)	−1.43(−3)	−1.68(−3)	−1.92(−3)	−2.17(−3)	−2.32(−3)	
102.2	−7.51(−4)	−9.17(−4)	−1.10(−3)	−1.28(−3)	−1.46(−3)	−1.62(−3)	
153.3	−3.51(−4)	−4.49(−4)	−5.38(−4)	−6.48(−4)	−7.47(−4)	−8.51(−4)	
204.4	−1.99(−4)	−2.54(−4)	−3.22(−4)	−3.91(−4)	−4.57(−4)	−5.25(−4)	

[a]Based upon tabulated internal-conversion matrix elements of Refs. 29 and 30.

going from $E1 \rightarrow E2$, $r_{\mu\mu'}$ is decreased by (kr), but $R_{\mu\mu'}$ is increased by $(kr)^{-1}$ which just offsets the decrease of $r_{\mu\mu'}$.

The suppression of $\xi_K(M1)$ occurs because of the suppression of the $r_{\mu\mu'}(M1)$ matrix element. In a nonrelativistic approximation $r_{\mu\mu'}(M1)$ is proportional to $\langle \mu \| \vec{\mathrm{M}} \| \mu' \rangle$ where $\vec{\mathrm{M}}$ is the magnetic moment operator. However, $\langle \mu \| \mathrm{M} \| \mu' \rangle = 0$ since the states do not belong to the same fine-structure multiplet. On the other hand, for high Z ($Z=83$), where such nonrelativistic approximations are no longer accurate, we see that $\xi_K(M1) \sim \xi_K(E2)$. All of these considerations also hold for the outer shells.

In Fig. 2(b) we plot ξ_K as a function of Z for $E_\gamma = 50$ keV and $E_\gamma = 130$ keV. We see that ξ_K usually increases rapidly with Z as we would expect since both the photoelectric and conversion effects gen-

TABLE III. L-shell contribution to conversion screening parameter.[a]

E_γ (keV)	$Z=73$	$Z=77$	$Z=81$	$Z=84$	$Z=88$	$Z=92$	Multipolarity
25.6	−3.67(−2)	−4.38(−2)	−5.07(−2)	−5.58(−2)	−6.28(−2)	−7.48(−2)	$\xi_L(E1)$
51.1	−1.07(−2)	−1.29(−2)	−1.53(−2)	−1.71(−2)	−1.98(−2)	−2.28(−2)	
76.7	−5.06(−3)	−6.11(−3)	−7.27(−3)	−8.26(−3)	−9.74(−3)	−1.13(−2)	
102.2	−2.93(−3)	−3.57(−3)	−4.28(−3)	−4.87(−3)	−5.79(−3)	−6.77(−3)	
153.3	−1.33(−3)	−1.62(−3)	−1.98(−3)	−2.26(−3)	−2.73(−3)	−3.22(−3)	
204.4	−7.60(−4)	−9.33(−4)	−1.14(−3)	−1.32(−3)	−1.59(−3)	−1.90(−3)	
25.6	−5.29(−4)	−6.99(−4)	−9.46(−4)	−1.29(−3)	−2.05(−3)	−3.07(−3)	$\xi_L(M1)$
51.1	−4.40(−4)	−6.00(−4)	−8.21(−4)	−1.03(−3)	−1.39(−3)	−1.89(−3)	
76.7	−3.74(−4)	−4.95(−4)	−6.64(−4)	−8.42(−4)	−1.14(−3)	−1.54(−3)	
102.2	−3.33(−4)	−4.40(−4)	−5.84(−4)	−7.31(−4)	−9.82(−4)	−1.33(−3)	
153.3	−2.54(−4)	−3.48(−4)	−4.70(−4)	−5.89(−4)	−8.00(−4)	−1.08(−3)	
204.4	−2.26(−4)	−2.95(−4)	−3.89(−4)	−4.82(−4)	−6.58(−4)	−8.82(−4)	
25.6	+9.55(−3)	+1.70(−2)	+2.74(−2)	+3.42(−2)	+4.65(−2)	+6.14(−2)	$\xi_L(E2)$
51.1	−2.46(−3)	−1.92(−3)	−1.01(−3)	−6.13(−5)	+1.64(−3)	+3.82(−3)	
76.7	−2.50(−3)	−2.54(−3)	−2.48(−3)	−2.26(−3)	−1.79(−3)	−1.30(−3)	
102.2	−1.72(−3)	−1.80(−3)	−1.79(−3)	−1.82(−3)	−1.64(−3)	−1.40(−3)	
153.3	−9.35(−4)	−1.03(−3)	−1.10(−3)	−1.14(−3)	−1.16(−3)	−1.13(−3)	
204.4	−5.95(−4)	−6.62(−4)	−7.17(−4)	−7.45(−4)	−7.75(−4)	−7.66(−4)	

[a]Based upon tabulated internal-conversion matrix elements of Refs. 29 and 30.

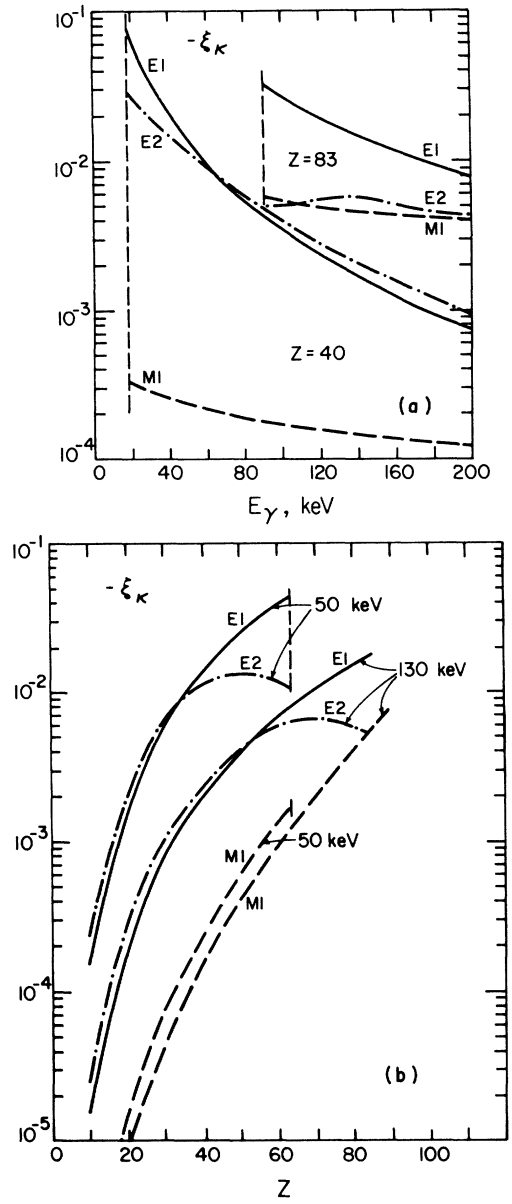

FIG. 2. (a) K-shell conversion screening parameter ξ_K vs the transition energy E_γ for $Z=40$ and $Z=83$ for $E1$, $E2$, and $M1$ multipole transitions. (b) ξ_K vs the nuclear charge Z for $E_\gamma=50$ keV and for $E_\gamma=130$ keV.

erally increase rapidly with Z. The maximum in the $\xi_K(E2)$ curves again is due to a peaking of the *partial* photoelectric cross section $\sigma_{pe}(E2)$. We also see again that for low Z we have $\xi_K(E2) \sim \xi_K(E1) \gg \xi_K(M1)$ for the reasons discussed above, while for high Z we have $\xi_K(M1) \sim \xi_K(E2)$ and as we see, the $M1$ contribution can even dominate.

Finally, we note that in all the cases given in Fig. 2 and Table I, ξ_K is negative so that the resulting dispersion term in Eq. (8) leads to an enhanced absorption cross section on the high-frequency side of resonance.

In Fig. 3 we plot the L-shell results $\xi_L(E1)$, $\xi_L(M1)$, and $\xi_L(E2)$ as functions of E_γ for $Z=81$, and also $\xi_L(E2)$ for $Z=92$. Comparing Figs. 3 and 2(a), or Tables I–III, we see that the L-shell contribution ξ_L is about (15–30)% as large as ξ_K in the energy region where the K shell is open. An interesting feature of the L-shell results for the high-Z cases shown is the change of sign of the $E2$ contribution, $\xi_L(E2)$ being positive for low energies, and negative for high energies. Comparing the curves for $\xi_L(E2)$ for $Z=81$ and $Z=92$, we see that the crossover energy where $\xi_L(E2)$ changes sign increases with increasing Z. Thus for low-energy high-Z $E2$ transitions in which the K shell is closed, ξ should be positive, leading to an enhanced total cross section on the low-frequency side of resonance in contrast to the usual case. As we will see in Sec. V, there is some experimental evidence of this behavior.

B. Rayleigh screening

Using the relativistic radial densities $\rho(r)$ of Mann,[34,35] we have calculated the Thomson contribution to the Rayleigh screening parameters ξ_R

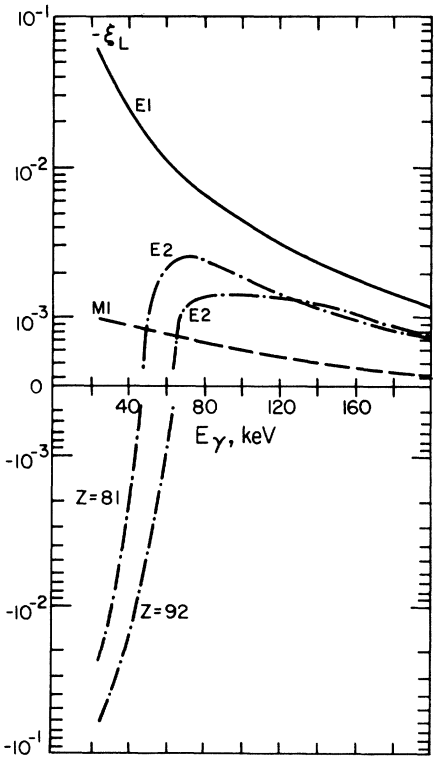

FIG. 3. Plots of the L-shell contribution ξ_L to the conversion screening parameter vs E_γ for $Z=81$ for $E1$, $E2$, and $M1$ transitions, and for $Z=92$ for $E2$ transitions.

TABLE IV. Thomson contribution to screening parameter.

E_γ (keV)	$Z=10$	$Z=20$	$Z=30$	$Z=40$	$Z=50$	$Z=60$	$Z=70$	$Z=80$	$Z=90$	Multipolarity
10	−9.74(−4)	−8.52(−4)	−1.41(−3)	−2.03(−3)	−2.56(−3)	−3.14(−3)	−3.88(−3)	−4.57(−3)	−5.18(−3)	$\xi_R(E1)$
20	−4.11(−4)	−1.04(−3)	−1.70(−3)	−2.44(−3)	−3.31(−3)	−4.10(−3)	−4.93(−3)	−5.87(−3)	−6.87(−3)	
30	−4.28(−4)	−1.04(−3)	−1.81(−3)	−2.60(−3)	−3.48(−3)	−4.46(−3)	−5.47(−3)	−6.47(−3)	−7.51(−3)	
40	−4.21(−4)	−1.03(−3)	−1.79(−3)	−2.68(−3)	−3.57(−3)	−4.54(−3)	−5.63(−3)	−6.79(−3)	−7.93(−3)	
60	−3.78(−4)	−1.02(−3)	−1.73(−3)	−2.61(−3)	−3.61(−3)	−4.63(−3)	−5.68(−3)	−6.85(−3)	−8.16(−3)	
80	−3.32(−4)	−9.84(−4)	−1.69(−3)	−2.51(−3)	−3.48(−3)	−4.57(−3)	−5.70(−3)	−6.87(−3)	−8.13(−3)	
100	−2.93(−4)	−9.27(−4)	−1.65(−3)	−2.45(−3)	−3.36(−3)	−4.42(−3)	−5.60(−3)	−6.85(−3)	−8.14(−3)	
120	−2.60(−4)	−8.67(−4)	−1.60(−3)	−2.39(−3)	−3.27(−3)	−4.28(−3)	−5.43(−3)	−6.72(−3)	−8.10(−3)	
140	−2.34(−4)	−8.08(−4)	−1.53(−3)	−2.34(−3)	−3.21(−3)	−4.18(−3)	−5.28(−3)	−6.56(−3)	−7.97(−3)	
160	−2.12(−4)	−7.55(−4)	−1.47(−3)	−2.27(−3)	−3.15(−3)	−4.10(−3)	−5.17(−3)	−6.40(−3)	−7.82(−3)	
180	−1.94(−4)	−7.07(−4)	−1.40(−3)	−2.21(−3)	−3.08(−3)	−4.03(−3)	−5.07(−3)	−6.27(−3)	−7.66(−3)	
200	−1.79(−4)	−6.63(−4)	−1.34(−3)	−2.13(−3)	−3.01(−3)	−3.96(−3)	−5.00(−3)	−6.17(−3)	−7.53(−3)	
10	−1.42(−4)	−1.95(−4)	−3.85(−4)	−4.06(−4)	−5.32(−4)	−6.30(−4)	−7.70(−4)	−8.21(−4)	−8.60(−4)	$\xi_R(M1)$
20	−1.61(−4)	−3.63(−4)	−5.69(−4)	−8.67(−4)	−9.80(−4)	−1.15(−3)	−1.49(−3)	−1.77(−3)	−1.92(−3)	
30	−1.72(−4)	−4.83(−4)	−6.86(−4)	−1.01(−3)	−1.37(−3)	−1.56(−3)	−1.83(−3)	−2.21(−3)	−2.61(−3)	
40	−1.96(−4)	−5.04(−4)	−8.14(−4)	−1.09(−3)	−1.51(−3)	−1.89(−3)	−2.19(−3)	−2.51(−3)	−2.91(−3)	
60	−2.33(−4)	−4.93(−4)	−8.99(−4)	−1.29(−3)	−1.64(−3)	−2.07(−3)	−2.57(−3)	−3.05(−3)	−3.46(−3)	
80	−2.41(−4)	−5.09(−4)	−8.74(−4)	−1.35(−3)	−1.79(−3)	−2.19(−3)	−2.64(−3)	−3.19(−3)	−3.77(−3)	
100	−2.35(−4)	−5.34(−4)	−8.56(−4)	−1.32(−3)	−1.84(−3)	−2.31(−3)	−2.74(−3)	−3.24(−3)	−3.82(−3)	
120	−2.22(−4)	−5.51(−4)	−8.59(−4)	−1.28(−3)	−1.81(−3)	−2.36(−3)	−2.85(−3)	−3.33(−3)	−3.85(−3)	
140	−2.07(−4)	−5.58(−4)	−8.73(−4)	−1.26(−3)	−1.76(−3)	−2.34(−3)	−2.90(−3)	−3.42(−3)	−3.93(−3)	
160	−1.93(−4)	−5.56(−4)	−8.87(−4)	−1.25(−3)	−1.72(−3)	−2.28(−3)	−2.88(−3)	−3.47(−3)	−4.02(−3)	
180	−1.80(−4)	−5.47(−4)	−8.98(−4)	−1.26(−3)	−1.69(−3)	−2.23(−3)	−2.84(−3)	−3.47(−3)	−4.07(−3)	
200	−1.68(−4)	−5.35(−4)	−9.03(−4)	−1.26(−3)	−1.67(−3)	−2.18(−3)	−2.78(−3)	−3.44(−3)	−4.09(−3)	
10	−9.21(−5)	−1.30(−4)	−2.43(−4)	−2.62(−4)	−3.41(−4)	−4.04(−4)	−4.87(−4)	−5.22(−4)	−5.47(−4)	$\xi_R(E2)$
20	−1.20(−4)	−2.44(−4)	−3.99(−4)	−5.69(−4)	−6.62(−4)	−7.75(−4)	−9.93(−4)	−1.16(−3)	−1.26(−3)	
30	−1.30(−4)	−3.26(−4)	−4.92(−4)	−7.08(−4)	−9.20(−4)	−1.07(−3)	−1.28(−3)	−1.52(−3)	−1.75(−3)	
40	−1.44(−4)	−3.58(−4)	−5.73(−4)	−7.94(−4)	−1.05(−3)	−1.29(−3)	−1.54(−3)	−1.78(−3)	−2.03(−3)	
60	−1.67(−4)	−3.77(−4)	−6.47(−4)	−9.29(−4)	−1.21(−3)	−1.49(−3)	−1.82(−3)	−2.16(−3)	−2.48(−3)	
80	−1.76(−4)	−3.90(−4)	−6.61(−4)	−9.83(−4)	−1.31(−3)	−1.62(−3)	−1.94(−3)	−2.31(−3)	−2.71(−3)	
100	−1.77(−4)	−4.03(−4)	−6.64(−4)	−9.93(−4)	−1.35(−3)	−1.71(−3)	−2.05(−3)	−2.41(−3)	−2.81(−3)	
120	−1.73(−4)	−4.12(−4)	−6.69(−4)	−9.90(−4)	−1.36(−3)	−1.75(−3)	−2.12(−3)	−2.50(−3)	−2.89(−3)	
140	−1.66(−4)	−4.18(−4)	−6.74(−4)	−9.86(−4)	−1.35(−3)	−1.75(−3)	−2.16(−3)	−2.57(−3)	−2.97(−3)	
160	−1.59(−4)	−4.19(−4)	−6.80(−4)	−9.84(−4)	−1.34(−3)	−1.74(−3)	−2.17(−3)	−2.60(−3)	−3.03(−3)	
180	−1.50(−4)	−4.16(−4)	−6.84(−4)	−9.83(−4)	−1.33(−3)	−1.73(−3)	−2.16(−3)	−2.61(−3)	−3.07(−3)	
200	−1.43(−4)	−4.12(−4)	−6.86(−4)	−9.83(−4)	−1.32(−3)	−1.71(−3)	−2.14(−3)	−2.60(−3)	−3.08(−3)	

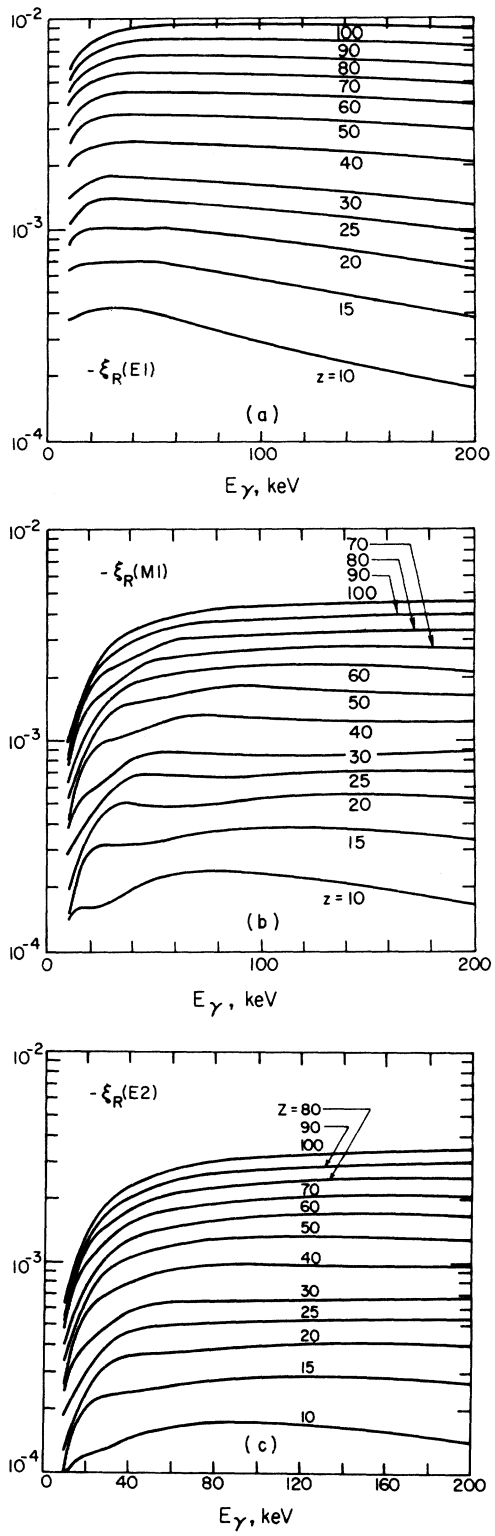

FIG. 4. (a) Thomson contribution to the Rayleigh screening parameter $\xi_R(E1)$ vs E_γ for various Z. (b) $\xi_R(M1)$ vs E_γ for various Z. (c) $\xi_R(E2)$ vs E_γ for various Z.

[Eqs. (16) and (17)]. We tabulate in Table IV our results for $E1$, $M1$, and $E2$ nuclear transitions, for Z varying from 10 to 90, and for E_γ ranging from 10–200 keV.

In Fig. 4(a)–4(c) we plot these results as functions of E_γ for various values of Z. Following an initial sharp rise in the low-energy region [where $\xi_R(EL, ML-1) \propto E_\gamma^{(2L-1)}$], ξ_R is then nearly constant in the region $E_\gamma \sim 20$–200 keV. At higher energies ($E_\gamma \gg Z\hbar c/a_0$), ξ_R will decrease $\propto 1/E_\gamma$. Comparing the various multipolarities, we see that the magnitude $\xi_R(E1)$ is greater than that of $\xi_R(M1)$, which in turn is larger than the magnitude of $\xi_R(E2)$. Comparing with the K- and L-shell conversion parameters plotted in Figs. 2 and 3, we see that in the high-energy region $E_\gamma \gtrsim 60$ keV, the Rayleigh contributions are about the same magnitude as the L-shell conversion contributions, and for an $M1$ transition, ξ_R can even dominate the K-shell conversion contribution. In the low-energy region, the Rayleigh contributions are generally much smaller than the conversion contribution.

We also note that in all cases $\xi_R < 0$, so that there is a net constructive interference between Rayleigh scattering and resonant scattering on the high-frequency side of resonance, and we see that the Rayleigh contribution adds constructively to the conversion contribution except for some cases of low-energy high-Z $E2$ transitions for which $\xi_L > 0$.

V. COMPARISON WITH EXPERIMENT

In Table V we list the various transitions for which experimental determinations of ξ have been made.[1,2,8-12,21] We also include the theoretical values of ξ_K, ξ_L, and ξ_R, the experimentally determined ξ_{expt} and our corresponding quantity ξ_{theory}.

Values for the K-shell contribution to conversion screening ξ_K were directly calculated for each Z, E_γ case. For the Thomson contribution to Rayleigh screening ξ_R, values appropriate to the E_γ of the transition were calculated for the four values of Z in Table IV closest to the transition Z. Lagrangian interpolation was then used to obtain ξ_R for the desired transition Z. These values of ξ_K and ξ_R should be reliable to within a few percent. For the L-shell conversion screening term ξ_L, on the other hand, values were obtained as needed by performing two-dimensional bicubic spline interpolations within Tables II and III. In some $E2$ cases these values should only be considered as estimates.

For pure multipole transitions, the theoretical value of ξ presented is then $\xi = \xi_K + \xi_L + \xi_R$. For the mixed $M1$-$E2$ transitions we give $\xi = [\xi(M1) + \delta^2 \xi(E2)]/(1+\delta^2)$, where δ^2 is the experimentally

TABLE V. Comparison of experimental and calculated interference parameters ξ for various γ-ray transitions.

Isotope	E_γ (keV)	Multipolarity	$100\xi_K$	$100\xi_L$	$100\xi_R$	$100\xi_{\text{theory}}$	$100\xi_{\text{expt}}$
$^{57}_{26}$Fe	14.4	$M1$	−0.007	a	−0.04	−0.05 [a]	···
$^{73}_{32}$Ge	13.3	$E2$	−3.32	a	−0.03	−3.4 [a]	−4.7 ± 1.0
$^{99}_{44}$Ru	90.0	$E2$ + 37% $M1$	−0.58($E2$) −0.03($M1$)	−.07($E2$) −.003($M1$)	−0.11($E2$) −0.15($M1$)	−0.60 [a] $\Delta\xi$ = −0.58 [c]	−0.33 ± 0.32 $\Delta\xi$ = −0.43 ± 0.50
$^{153}_{63}$Eu	97.4	$E1$	−1.36	−0.19	−0.48	−2.03	−1.1 ± 0.3
$^{155}_{64}$Gd	86.5	$E1$	−1.77	−0.26	−0.50	−2.53	−2.5 ± 0.5
	105.3	$E1$	−1.23	−0.17	−0.48	−1.88	−1.8 ± 0.5
$^{161}_{66}$Dy	25.6	$E1$	0	−2.74	−0.49	−3.23	−3.5 ± 0.5
	74.5	$E1$	−2.50	−0.39	−0.53	−3.42	−3.0 ± 0.5
$^{166}_{68}$Er	80.6	$E2$	−0.92	−0.21	−0.19	−1.32	−1.60 ± 0.19
$^{170}_{70}$Yb	84.3	$E2$	−0.87	−0.21	−0.20	−1.28	−1.70 ± 0.38
$^{171}_{70}$Yb	66.7	$M1$ + 49% $E2$	−1.05($E2$) −0.21($M1$)	−0.25($E2$) −0.03($M1$)	−0.19($E2$) −0.26($M1$)	−0.83 [c]	−1.00 ± 0.14
$^{180}_{72}$Hf	93.3	$E2$	−0.82	−0.19	−0.21	−1.22	−1.82 ± 0.48
$^{181}_{73}$Ta	6.3	$E1$	0	0	−0.32	−19.1ϵ [b]	−15.5 ± 0.5
$^{182}_{74}$W	100.1	$E2$	−0.77	−0.18	−0.22	−1.17	−1.0 ± 0.1
$^{183}_{74}$W	99.1	$E2$	−0.77	−0.18	−0.22	−1.17	−1.25 ± 0.17
	46.5	$M1$ + 0.6% $E2$	0	−0.05($M1$) −0.3($E2$) [d]	−0.25($M1$) −0.18($E2$)	−0.3 [c,d]	−0.05 ± 0.06
$^{184}_{74}$W	111.1	$E2$	−0.75	−0.16	−0.22	−1.13	−1.53 ± 0.29
$^{186}_{74}$W	122.5	$E2$	−0.71	−0.14	−0.23	−1.08	−2.09 ± 0.36
$^{186}_{76}$Os	137.2	$E2$	−0.64	−0.12	−0.24	−1.00	−1.02 ± 0.25
$^{188}_{76}$Os	155.0	$E2$	−0.57	−0.10	−0.24	−0.91	−1.51 ± 0.49
$^{191}_{77}$Ir	129.5	$M1$ + 14% $E2$	−0.31($M1$) −0.66($E2$)	−0.04($M1$) −0.13($E2$)	−0.32($M1$) −0.24($E2$)	−0.71	−0.50 ± 0.12
$^{193}_{77}$Ir	73.1	$M1$ + 31% $E2$	0	−0.05($M1$) −0.25($E2$)	−0.30($M1$) −0.22($E2$)	$\Delta\xi$ = −0.12 [c]	$\Delta\xi$ = +0.11 ± 0.38
$^{197}_{79}$Au	77.3	$M1$ + 12.1% $E2$	0	−0.06($M1$) −0.25($E2$)	−0.31($M1$) −0.23($E2$)	−0.38 [c]	−0.414 ± 0.017
$^{236}_{92}$U	45.3	$E2$	0	+0.8 [d]	−0.22	+0.6 [d]	+0.25 ± 0.75

[a] For these cases ξ_L was not calculated and is omitted from ξ_{theory}. We should expect $\xi_L \approx (0.1 - 0.3)\xi_K$.
[b] Calculated using the estimate of Eq. (15).
[c] For mixed $M1$-$E2$ transitions, $\xi = [\xi(M1) + \delta^2\xi(E2)]/(1+\delta^2)$ and $\Delta\xi = \xi(E2) - \xi(M1)$.
[d] The interpolated $\xi_L(E2)$ values for these two transitions are less certain due to the rapid variation of ξ_L in the energy region concerned.

determined $E2/M1$ mixing ratio. For the 90-keV ^{99}Ru transition and the 73-keV ^{193}Ir transition we also give $\Delta\xi = \xi(E2) - \xi(M1)$ which is the quantity measured indirectly in the time reversal invariance experiments.[1-3,22,23]

For the 6-keV $E1$ transition of ^{181}Ta, both the K and L shells are closed to conversion, and here the theoretical value of ξ given is that determined by the approximate formula (15), ξ_R being much smaller. As an example of a low-energy $M1$ transition, we also give our calculated values of ξ for the 14.4-keV $M1$ transition of ^{57}Fe, although here there has been no experimental determination of ξ.

The agreement between experiment and theory is reasonably good. In almost all cases the theoretical value of ξ lies within or just at the quoted error limits.

We also note that in many cases, our theoretical values are somewhat smaller in magnitude than the corresponding experimental values. We expect that the magnitude of theoretical values would be increased a small amount by inclusion of outer shell contributions (primarily M and N) to the conversion screening, leading to a general improvement between theory and experiment.

As a particular example, for the 13.3-keV $E2$ transition of ^{73}Ge, we would expect the combined contributions from the L and M shells to be about (15–30)% of the ξ_K contribution, leading to a theoretical value $\xi \sim -4 \times 10^{-2}$, in much better agreement with experiment. In most of the other cases, L-shell conversion screening is already included,

and the increases would be much less pronounced [perhaps (15–30)% of ξ_L].

The strongest discrepancies occur for the 97.4-keV ^{153}Eu $E1$ transition, the 46.5-keV ^{183}W $M1$ transition, and the 122.5-keV ^{186}W $E2$ transition, where in all these cases the calculated value is several times too large or too small. The origin of the disagreement between theory and experiment in these cases is not clear.

It is also interesting to note the relative magnitude of the various screening contributions. Examining the table, we see that the L-shell conversion contribution ξ_L is roughly (15–30)% of the K-shell contribution ξ_K when the K shell is open, and that in the energy region $E_\gamma > 50$ keV the Rayleigh contribution ξ_R is usually somewhat larger than ξ_L, being roughly (25–50)% ξ_K. In a case such as the 77.3-keV transition of ^{197}Au, the K shell is closed and the dominant contribution to ξ is then Rayleigh screening. This is also the case for a low-energy $M1$ transition such as ^{57}Fe where there is a strong suppression of conversion screening.

An interesting special case is the 45.3-keV $E2$ transition of $^{236}_{92}$U. Here the K shell is closed to conversion, and, as shown in Fig. 3, in this energy region the L-shell conversion contribution is positive, $\xi_L \simeq +0.8\times10^{-2}$. This contribution adds destructively to the Rayleigh contribution $\xi_R \simeq -0.2\times10^{-2}$ to give a net positive screening parameter $\xi \simeq +0.6\times10^{-2}$. This leads to an enhanced total cross section on the low-frequency side of resonance in contrast to the usual case. This predicted positive sign of ξ agrees with the median of the experimental value $\xi_{expt} = (+0.25\pm0.75)\times10^{-2}$, but here the error bars are too large to verify the change of sign.

VI. SUMMARY

This paper presents the first extensive calculations of the interference parameters arising in low-energy γ-ray optics. Although these represent small effects, they can be quite important in precise isomer shift determinations and in analyzing γ-ray time-reversal invariance tests. The interference parameters should also be of interest for fundamental atomic physics calculations since, for an $M1$ or $E2$ nuclear transition, they effectively isolate higher multipole contributions from predominantly $E1$ electronic scattering and absorption processes.

The dominant screening contributions are the conversion screening, given by Eqs. (10) and (11), and the Thomson contribution to Rayleigh screening, given by Eqs. (16) and (17). Our main results are calculations of these contributions for $E1$, $M1$, and $E2$ multipolarities for various Z and E_γ which are presented in Tables I–IV. These results are compared with the available experiments in Table V.

Among the interesting features that emerge is that for conversion screening there is only a weak dependence on the multipolarity of the nuclear transition. In particular, we find that $\xi_c(E2) \sim \xi_c(E1)$, and more generally, $\xi_c(EL) \sim \xi_c(E1)$. For $M1$ transitions, we find that $\xi_c(M1)$ is suppressed for low-energy transitions ($E_\gamma \lesssim 100$ keV) in low-Z nuclei ($Z \lesssim 50$), but at higher energies and higher Z, $M1$ conversion screening can be just as pronounced as $E1$ or $E2$ screening.

In most cases we find that conversion screening dominates Rayleigh screening, but that Rayleigh screening is still significant, and for low-energy $M1$ transitions and in cases where the K shell is closed to conversion, ξ_R can even be the dominant contribution.

One other point of interest is that in almost all cases the screening parameter ξ is found to be negative, leading to an enhanced total absorption cross section on the high-frequence side of resonance, but in low-energy high-Z $E2$ transitions in which the K shell is closed this behavior should be reversed.

Note added in proof. The interference parameters have recently been determined for two more Mössbauer transitions by Poetzel *et al.*[36] For the 59.5 keV, $E1$ transition of $_{93}$Np^{237}, they measured $\xi_{exp} = -(3.4\pm0.2)\times10^{-2}$, and for the 98.7 keV, $M1$ transition of $_{78}$Pt^{195} they measured $\xi_{exp} = -(1.1\pm0.3)\times10^{-2}$. Our theoretical calculations for these cases are for Np^{237}: $100\xi_K = 0$, $100\xi_L = -2.10$, $100\xi_R = -0.84$, giving $\xi_{theory} = -2.94\times10^{-2}$; and for Pt^{195}: $100\xi_K = -0.37$, $100\xi_L = -0.05$, $100\xi_R = -0.32$, giving $\xi_{theory} = -0.74\times10^{-2}$.

ACKNOWLEDGMENTS

We wish to acknowledge useful conversations with Professor G. T. Trammell and with Dr. Peter Herczeg. We also wish to thank Dr. J. B. Mann for allowing us to use some of his unpublished radial density results, and Dr. Loren Pfeiffer for sending us the results of his measurement of the interference effects in ^{73}Ge prior to publication.

APPENDIX

For reference, we give the expressions for the partial cross sections for the EL and ML contributions to photoelectric absorption and Thomson scattering.

The ML and EL multipole contributions to the photoelectric absorption cross sections are given by

$$\sigma_e(ML) = 2(\pi\lambda\!\!\!^{-}_0)^2\alpha k[L(L+1)]^{-1}\sum_{\mu\mu'} B_{\mu\mu'}\gamma_{\mu\mu'}(m)^2, \quad \text{(A1)}$$

$$\sigma_e(EL) = 2(\pi\lambda\!\!\!^{-}_0)^2 \alpha k[L(L+1)]^{-1} \sum_{\mu\mu'} C_{\mu\mu'} r_{\mu\mu'}(e)^2, \quad \text{(A2)}$$

where the notation is that used in Eqs. (10) and (11).

The partial cross-section contributions to the Thomson scattering cross section (elastic and inelastic) are given by

$$\sigma_R(ML) = \pi(4L+2)(Zr_0)^2 \langle j_L^2(k_0 r)\rangle^2, \quad \text{(A3)}$$

$$\sigma_R(EL) = \pi(4L+2)(Zr_0)^2 \left\langle \left(\frac{L+1}{2L+1}\right) j_{L-1}^2(k_0 r) + \left(\frac{L}{2L+1}\right) j_{L+1}^2(k_0 r) \right\rangle^2, \quad \text{(A4)}$$

where the notation is that used in Eqs. (16) and (17).

---

*Work supported in part by the NSF.

[1]O. C. Kistner, Phys. Rev. Lett. 19, 872 (1967).

[2]M. Atac, B. Chrisman, P. Debrunner, and H. Frauenfelder, Phys. Rev. Lett. 20, 691 (1968).

[3]J. P. Hannon and G. T. Trammell, Phys. Rev. Lett. 21, 726 (1968).

[4]C. Sauer, E. Matthias, and R. L. Mössbauer, Phys. Rev. Lett. 21, 961 (1968).

[5]G. T. Trammell and J. P. Hannon, Phys. Rev. 180, 337 (1969).

[6]J. P. Hannon and G. T. Trammell, Phys. Rev. 186, 306 (1969).

[7]Yu. Kagan, A. M. Afanas'ev, and V. K. Voitovetskii, Zh. Eksp. Teor. Fiz. Pis'ma Red. 9, 155 (1969) [JETP Lett. 9, 91 (1969)].

[8]D. V. Gorobchenko, I. I. Lukashevich, V. V. Sklyarevskii, and N. I. Filippov, Zh. Eksp. Teor. Fiz. Pis'ma Red. 9, 237 (1969) [JETP Lett. 9, 139 (1969)].

[9]W. Henning, G. Bähre, and P. Kienle, Phys. Lett. B 31, 203 (1970).

[10]F. E. Wagner, B. D. Dunlap, G. M. Kalvius, H. Schaller, R. Felscher, and H. Spieler, Phys. Rev. Lett. 28, 530 (1972).

[11]D. J. Erickson, J. F. Prince, and L. D. Roberts, Phys. Rev. C 8, 1916 (1973).

[12]Loren Pfeiffer, Phys. Rev. Lett. 38, 862 (1977).

[13]A. M. Afanas'ev and Yu. Kagan, Phys. Lett. A 31, 38 (1970).

[14]K. P. Mitrofanov, M. V. Plotnikova, N. I. Rokhlov, and V. S. Shpinel', Zh. Eksp. Teor. Fiz. Pis'ma Red. 12, 85 (1970) [JETP Lett. 12, 60 (1970)].

[15]I. I. Lukashevich, V. P. Gorobchenko, V. V. Skylarevskii, and N. I. Filippov, Phys. Lett. A 31, 112 (1970).

[16]P. Steiner and G. Weyer, Phys. Lett. A 36, 201 (1971); Z. Phys. 248, 362 (1971).

[17]P. J. Black and P. B. Moon, Nature (Lond.) 188, 481 (1960).

[18]P. B. Moon, Proc. R. Soc. A 263, 309 (1961).

[19]P. J. Black, D. E. Evans, and D. A. O'Connor, Proc. R. Soc. A 270, 168 (1962).

[20]F. Hartmann-Boutron and D. Spanjaard, J. Phys. (Paris) 38, 691 (1977).

[21]G. Kaindl, D. Salomon, and G. Wortmann, Phys. Rev. B 8, 1912 (1973).

[22]E. M. Henley, Ann. Rev. Nucl. Sci. 19, 367 (1969).

[23]J. P. Hannon, Nucl. Phys. A 177, 493 (1971).

[24]N. K. Cheung, H. E. Henrikson, E. J. Cohen, A. J. Becker, and F. Boehm, Phys. Rev. Lett. 37, 588 (1976).

[25]M. E. Rose, *Elementary Theory of Angular Momentum* (Wiley, New York, 1957), pp. 32–48.

[26]L. Tassie, *Report on the First Mössbauer Conference* (Allerton, Urbana, Ill., 1960).

[27]This terminology is somewhat misleading, since there is interference not only between the (coherent elastic) Rayleigh scattering from the atomic electrons and the coherent elastic resonant scattering from the nucleus, but also between quantum-mechanically coherent inelastic processes in which the crystal vibration state changes during the scattering.

[28]M. E. Rose, *Internal Conversion Coefficients* (North-Holland, Amsterdam, 1958).

[29]I. M. Band, M. A. Listengarten, and L. A. Sliv, in *Alpha-, Beta-, and Gamma-Ray Spectroscopy*, edited by K. Siegbahn (North-Holland, Amsterdam, 1965), Vol. II, p. 1673–1680.

[30]I. M. Band, M. A. Listengarten, and L. A. Sliv, in *Internal Conversion Processes*, edited by Joseph H. Hamilton (Academic, New York, 1966), p. 589.

[31]We note that the Rayleigh screening parameter $\xi_R(EL)$ given by Eq. (17) differs from the expression (23) given in Ref. 6. The latter expression was derived using the first (A^2) term of $E_{\mu\nu}$ given in Eq. (6) of Ref. 6. There is, however, an additional term contributed by the $T(j_\mu, j_4)$ term of $E_{\mu\nu}$ which just cancels out the longitudinal contribution of the A^2 term, yielding Eq. (17). It is easily verified by direct calculation of the interference term from the scattering amplitudes (4) and (5) that this expression for $\xi(EL)$ correctly accounts for the interference between Thomson and resonant scattering.

[32]See, e.g., R. W. James, *The Optical Principles of Diffraction of X-rays* (Cornell U.P., Ithaca, New York, 1965) pp. 135–193.

[33]M. E. Rose, in Ref. 29, Vol. II, Chap. XVI, p. 887.

[34]J. B. Mann, At. Data 5, 209 (1973).

[35]J. B. Mann (private communication).

[36]W. Poetzel, F. E. Wagner, G. M. Kalvius, L. Asch, J. C. Spirlet, and W. Müller, talk presented at the Mössbauer Symposium, Argonne, 1977, AIP Conf. Proc. (to be published).